NAL-Conf-74/66 EXP

Rockefeller University
COO-2232A-5

University of Rochester
COO-3065-88 (UR-495)

EXCITATION OF THE PROTON TO LOW MASS STATES AT 180 and 270 GeV

Y. Akimov, L. Golovanov, S. Mukhin, G. Takhtamyshev, and V. Tsarev

Joint Institute for Nuclear Research, Dubna, U.S.S.R.

E. Malamud, R. Yamada, P. Zimmerman

Fermi National Accelerator Laboratory, Batavia, Illinois

R. Cool, K. Goulianos, H. Sticker

Rockefeller University, New York, New York

D. Gross, A. Melissinos, D. Nitz, S. Olsen

University of Rochester, Rochester, New York

Excitation of the Proton to Low Mass States at 180 and 270 GeV

Y. Akimov, L. Golovanov, S. Mukhin, G. Takhtamyshev, and V. Tsarev

Joint Institute for Nuclear Research, Dubna, U.S.S.R.

E. Malamud, R. Yamada, P. Zimmerman

Fermi National Accelerator Laboratory, Batavia, Illinois

R. Cool, K. Goulianos, H. Sticker

Rockefeller University, New York, New York

D. Gross, A. Melissinos, D. Nitz, S. Olsen

University of Rochester, Rochester, New York

Paper submitted to the XVIIth International Conference on High Energy Physics, 1-10 July 1974, Imperial College, London.

ABSTRACT

We have used the gas jet target in the internal beam of the FERMILAB accelerator with the provision of a special slit in order to improve the resolution of the measurement of the angle of the recoil target particle in the reaction $p + d \rightarrow N^* + d$. This results in an improvement of the mass resolution so that it is possible to separate the $N^*(1400)$ and $N^*(1690)$ mass regions from the proton-deuteron elastic peak up to incident proton energies of 270 GeV. It is observed that the excitation cross section is independent of incident energy whereas the t-dependence is a strong function of the mass. Furthermore, the data agree with the corresponding reaction $p + p \rightarrow N^* + p$ when the deuteron form factor is taken into account.

I. Introduction

In an experiment performed at the Fermi National Accelerator Laboratory (FERMILAB), we studied the coherent, inclusive reaction

$$p + d \rightarrow X + d \qquad (1)$$

at incident momenta of 180 and 270 GeV/c my measuring low energy deuteron recoils from an internal deuterium gas jet target, in addition we obtained a limited amount of data on hydrogen. Here we report the results for those reactions where the mass of state X, M_x, is near the mass of the proton ($M_x < 2$ GeV/c^2) and where the four momentum transfer, t, is small ($.025 \leq |t| \leq .07$ (GeV/c)^2).

The related reaction

$$p + p \rightarrow X + p \qquad (2)$$

has been studied in this M_x and t region at lower energies[1-3]. At these energies (typically 10 - 30 GeV) the mass spectrum has considerable structure and a t behavior which varies drastically across this mass range. A broad resonance-like bump is observed at $M_x \sim 1.4$ GeV/c^2 whose production on protons is rapidly damped in t (approximately as $e^{-20|t|}$). Other structures with less severe t dependence have been reported at $M_x \approx 1.52$ and 1.69 GeV/c^2. The latter bumps are generally considered to be the excitation of resonant proton isobars, while the enhancement at 1.4 GeV/c^2 is somewhat more of a mystery. It has been variously interpreted as being either the effect of other resonant states or as threshold effects associated with π and $\Delta\pi$ production. A systematic

study of the s and t dependence of the cross section in this mass range may help resolve these questions.

II. Technique

Recoil deuterons from the jet target were detected using stacks of solid state detectors located in the main ring vacuum chamber of the FERMILAB Accelerator (see Fig. 1). The general features of this type of measurement are described in reference 4 and references cited therein and will not be repeated here. The special feature for these measurements was the improvement of the angular resolution by the introduction of a movable tungsten slit system near the gas jet target.

The mass resolution in this experiment is almost totally due to the uncertainty in the determination of recoil angle ω, and is given by

$$\Delta M_x^2 = 2P_o \sqrt{|t|} \quad \Delta\omega \qquad (3)$$

where P_o is the incident beam momentum. For an uncollimated jet $\Delta\omega \simeq \pm 3$ mrad, hence at $P_o = 300$ GeV/c and $|t| = .04$ $(\text{GeV/c})^2$ $\Delta M_x^2 = \pm .36$ $(\text{GeV/c}^2)^2$, so at $M_x = 1.4, \Delta M_x = \pm 130$ MeV/c^2. This resolution is not suitable for the desired low mass measurements. The inelastic states of interest are kinematically near the elastic scattering peak, and since inelastic scattering is typically a small fraction of elastic scattering, high resolution is necessary for achieving an unambiguous signal. Also high resolution is needed for the determination of structure and the separation of various peaks. Finally, the gas jet target is usually accompanied by a small amount of residual gas in the accelerator vacuum system, and in some cases elastic scattering from

this residual gas can reach the detector stacks, simulating an inelastic event. For these reasons the jet target was collimated. The effect of the slit in enhancing the mass resolution is clearly demonstrated in Fig. 2, where the elastic scattering peaks are shown with and without a slit. The data were obtained with the slit 4 mm wide, which matches the aperture of our detector collimators, in which case $\Delta\omega \simeq \pm 1.2$ mrad and for $P_o = 300$ (GeV/c), $t = 0.04$ $(GeV/c)^2$, $M_x = 1.4$ (GeV/c^2) we obtain $\Delta M_x = \pm 50$ MeV/c^2.

In the absence of the slit, elastic scattering detected in a fixed detector stack can be used to infer the luminosity of the target. This is not useful for a collimated jet because the slit introduces parallax effects which cause each detector to see different interaction regions in the target (see Fig. 1). Therefore our results had to be normalized to elastic scattering peaks observed in the same detector, limiting the mass and t range over which this technique is useful. For recoil masses near that of the proton m_p, the difference in recoil kinetic energy between elastic scattering and inelastic scattering at the same recoil angle is approximately

$$\Delta T \simeq \frac{M_x^2 - m_p^2}{P_o} \quad , \tag{4}$$

hence the technique is better suited for high incident beam energies where more masses appear in a narrow T-interval close to the elastic peak. Background from slit scattering was monitored by running a jet at low energy (50 GeV) where essentially no inelastic protons were produced over the useful recoil kinetic energy range covered by the detector. Counts in this region were attributed to background processes involving elastic recoils, such as slit scattering. Since elastic scattering changes only slightly from 50 to 300 GeV/c, these data could be used

as an estimate of background in the higher energy data (typically 10 to 20%). Figure 3 illustrates the kinetic energy spectra obtained for 50, 180 and 270 GeV/c incident momenta, with various mass values indicated.

III Data

From the corrected number of counts observed in a detector stack, N(t), in a t range Δt ($t = 2m_d T$) we determine the cross section according to the relation

$$\frac{d^2\sigma}{dt\,dM_x^2} = \frac{\pi}{P_o\sqrt{\left(\frac{t}{2m_d}\right)^2 + |t|}} \frac{1}{\Delta t} N(t) \left(\frac{d\sigma_{el}}{d\Omega} \frac{1}{N_{el}}\right) \qquad (5)$$

where N_{el} is the number of elastic counts observed in the detector and $d\sigma_{el}/d\Omega$ is the elastic differential cross section at the angle of the particular detector. For this we used:

$$\frac{d\sigma_{el}}{d\Omega} = \frac{\sigma_T^2}{16\pi^2} 2m_d\sqrt{|t_{el}|}\; e^{-b|t_{el}| + ct^2} \qquad (6)$$

where σ_T is the total cross section for pd scattering and b,c are the elastic pd "slope" parameters

$$b = 26.0 + b_{pp}\ (\mathrm{GeV/c})^{-2}$$
$$c = 60.0\ (\mathrm{GeV/c})^{-4} \qquad (7)$$

where $b_{pp} = 8.23 + .556$ ℓn s. This is what is expected from simple Glauber theory using a deuterium form factor as determined by Nikitin et al[5] and the p-p slope parameter as determined from an earlier gas jet experiment at FERMILAB.[6] For σ_T we used 73.4 mb at both energies, consistent with recently reported FERMILAB results.[7] Since each detector stack

defines a fixed angle the values for M_x^2 and t were correlated according to the relation

$$M_x^2 \simeq m_p^2 + 2P_o\sqrt{|t|}\left[\sin\omega - \left(\frac{P_o + m_d}{P_o}\right)\frac{\sqrt{|t|}}{2m_d}\right] \qquad (8)$$

(ω is measured relative to 90° from the beam direction as indicated in Fig. 1). Taking data in three detector stacks at a variety of angles enabled us to compile a matrix of cross sections vs. t and M_x^2 for incident momenta of 180 and 270 GeV/c. The error associated with each point was statistical and included the uncertainties associated with the background subtraction and normalization. It is important to note that the cross sections reported here are deuterium cross sections divided by a deuteron form factor squared

$$F_d(t) = \left(\frac{\sigma_{pd}}{\sigma_{pp}}\right)^2 e^{-26|t| + 60t^2} \qquad (9)$$

This was done to facilitate comparisons with data taken on hydrogen (reaction 2).

IV Results

The M_x^2 variation of the cross section is shown in Fig. 4 for three different t values. A peak is observed at $M_x^2 \simeq 2$ $(GeV/c^2)^2$ with another peak or shoulder at about $M_x^2 \simeq 2.9$. A difference in t dependence between the lower and higher masses is clearly evident. The data taken at the two energies are strikingly similar, indicating the absence or at most a very weak energy dependence. The point to point ratio taken where the two energies overlap yields

$$\left\langle \frac{d^2\sigma/dtdM_x^2\ (180\ GeV/c)}{d^2\sigma/dtdM_x^2\ (270\ GeV/c)} \right\rangle = 1.04 \pm .02$$

(For this ratio the extreme low mass data points are neglected since the (instrumental) background is strongly energy dependent for the mass region immediately adjacent to the elastic peak.)

We have parameterized the data for fixed M_x^2 as $A(M_x^2)\ e^{-b(M_x^2)t}$. The data points and the best fits for $M_x^2 = 1.8$ are shown in Fig. 5. The steep t dependence, $b(M_x^2=1.8) \simeq 22\ (\mathrm{GeV}/c)^{-2}$ persists at high energy and the cross-section continues to increase with decreasing t even at quite small t. The best fit values of A and b, as well as the production cross section integrated over t (i.e., $d\sigma/dM_x^2 \equiv \int dt\ d^2\sigma/dt dM_x^2 = A(M_x^2)/b(M_x^2)$) are shown in Fig. 6.

In view of the significant enhancement at $M_x^2 \simeq 2\ (\mathrm{GeV}/c^2)^2$, and the apparent shoulder at $M_x^2 \sim 2.9\ (\mathrm{GeV}/c^2)^2$, we have made a fit to the mass spectra (simultaneously at all values of t) using a Breit-Wigner resonance centered near $M_x^2 = 2\ (\mathrm{GeV}/c^2)^2$.

$$\frac{d^2\sigma}{dt dM_x^2} = \frac{1}{M_x}\ \frac{\Gamma^2\ C\ e^{-bt}}{4(M_x - M_r)^2 + \Gamma^2} \qquad (10)$$

where M_r and Γ are the "resonance" position and width to be determined by the fit. Similarly the constants C and b are determined by the fit. The isobar excitation cross section at $t = 0$ is obtained by integrating Eq. (10) and is related to the fit parameters through

$$\left(\frac{d\sigma}{dt}\right)_{t=0} = \Gamma C[\pi/2 + \tan^{-1}(2(M_r - M_T)/\Gamma)] \qquad (11)$$

where $M_T = 1.08\ (\mathrm{GeV}/c^2)$ is the pion production threshold.

In the fit we have not included any non-resonance background but in order to obtain a satisfactory fit it was necessary to include a second Breit-Wigner resonance centered in the vicinity of $M_x^2 = 2.9\ (\mathrm{GeV}/c^2)^2$. The parameters of this resonance were also determined by the fit. The

parameters of the $M_x^2 = 2.0\ (GeV/c^2)^2$ enhancement obtained through this procedure for an incident energy of 270 GeV are shown below. The quality of the fit is characterized by $\chi^2 = 124$ for 117 degrees of freedom.

$N^*(1400)$ parameters as determined from fit	
M_r (MeV)	1387 ± 10
Γ (MeV)	313 ± 25
$(d\sigma/dt)_{t=0}$ Mb/(GeV/c)^2	7.7 ± 0.5
b(GeV/c)$^{-2}$	19.0 ± 2.0

The curves in Fig. 4 are the results of the fit described above. Also, a similar fit is displayed in Fig. 7 where we show data from reaction (2) p + p → N* + p obtained with the same apparatus at an incident momentum $P_o = 385$ (GeV/c). Note, however, that the data in Fig. 7 are displayed at fixed angle so that different t-values correspond to different masses as shown. Finally, in Fig. 8 we show the fitted curve for $(d\sigma/dt)_{t=0}e^{-bt}$ (see Eq. 11) for $M_x^2 = 2.0\ (GeV/c^2)^2$ at the higher energy together with pp data points from references 1,2, 3 and some recent pp measurements at the FERMILAB[8]; the data points reported in this work are also shown. The agreement is good, showing the validity of factorizing the deuteron data in terms of pp data and the deuteron form factor.

V Conclusions

The bumps seen in the missing mass spectra persist at high energy and continue to rise at quite small t($t \sim .025\ (GeV/c)^2$), showing no indication of turning over. The energy independence of the cross-section for reactions 1 and 2 is a strong confirmation of the diffraction

dissociation ideas advanced by Feinberg and Pomeranchuk in 1956 and later by Good and Walker in 1960[10]. If this cross section depended on s to some power n, i.e., $d^2\sigma/dtdM_x^2 \propto s^{-n}$, then from these data alone $|n| \lesssim 0.15$, or if on the other hand the behavior is logarithmic, i.e., $d^2\sigma/dtdM_x^2 \propto A + B \ln s$, then this experiment yields $|B/A| \lesssim .15$. The lack of energy dependence is further substantiated when the low energy data[1-3] are taken into account.

VI Acknowledgments

We thank the many members of FERMILAB who supported our effort during the course of this experiment. We are also grateful to Mr. T. Haelen of the University of Rochester who designed the slit system and the members of the 130" cyclotron staff who manufactured and instrumented it on short notice. The Soviet members of the group would like, in addition, to express their deep gratitude to the State Committee for Utilization of Atomic Energy and to the Joint Institute for Nuclear Research (Dubna) for their generous assistance.

References and Footnotes

1. R. M. Edelstein, et al., Phys. Rev. D5, 1073 (1972).

2. G. Belletini, et al., Phys. Letters 18, 167 (1965).

3. J. V. Allaby et al., Nucl. Phys. B52, 316 (1973). This article summarizes previous work in the subject.

4. Y. Akimov et al., Proton-Deuteron Elastic Scattering and Diffraction Dissociation from 50 to 400 GeV, paper submitted to the XVIIth International Conference on High Energy Physics.

5. V. A. Nikitin et al., Preprint No. P1-7004, JINR, Dubna, USSR, 1973.

6. V. Bartenev et al., Phys. Rev. Letters 31, 1088 (1973). The "slope" given by Eq. (7) does not include the effects of rescattering. Since we later divide by the same form factor the rescattering effects tend to cancel in so far as they effect elastic and inelastic scattering in the same way.

7. W. Baker et al., to be published.

8. V. Bartenev et al., to be published.

9. The t-dependence for the enhancement at $M_x^2 \simeq 2.0\ (\mathrm{GeV}/c^2)^2$ shown in Fig. 8 is clearly dependent on the model used for the fit. It should be compared with Fig. (6a) where the b-values are model independent. Note that since we use the same form factor for normalization and the extraction of single nucleon cross sections, we are not very sensitive to the choice of the deuteron form factor (Eq. 9).

10. E. L. Feinberg, I. Pomeranchuk, Suppl. Nuovo Cimento, 3, 652 (1956); M. L. Good and W. D. Walker, Phys. Rev. 120, 1857 (1960).

Figure Captions

1. Schematic drawing ofthe experimental arrangement, indicating the parallax effects caused by the slit.
2. Elastic peaks observed with the slit; a) wide open and b) closed to a 4 mm aperture.
3. Recoil energy spectra observed in a detector stack with the three incident energies superimposed. Pion threshold at 50 GeV is indicated together with the corresponding masses at the higher energies.
4. $d^2\sigma/dtdM_x^2$ vs. M_x^2 at $|t| = .027$, .039, and .051 $(GeV/c)^2$. The curves are Breit-Wigner resonance fits to the higher energy data as described in the text.
5. $d^2\sigma/dtdM_x^2$ vs. t for $M_x^2 = 1.8$ $(GeV/c^2)^2$.
6. a) The slope parameter b vs. M_x^2. The observed variation of b with M_x^2 may be less fast than in reality due to our finite mass resolution.

   b) The parameter A vs. M_x^2.

   c) $d\sigma/dM_x^2$ $(= A(M_x^2)/b(M_x^2))$ vs. M_x^2 .
7. $d^2\sigma/dtdM_x^2$ for the reaction $p + p \rightarrow X + p$ at 385 GeV and $|t| = .02$ $(GeV/c)^2$.
8. Small t data on the reaction $pp \rightarrow N^* + p$ compared with our 270 GeV fit for $N^*(1400)$ production. The pd points on the plot are results of separate fits with two Breit-Wigners at each value of t.

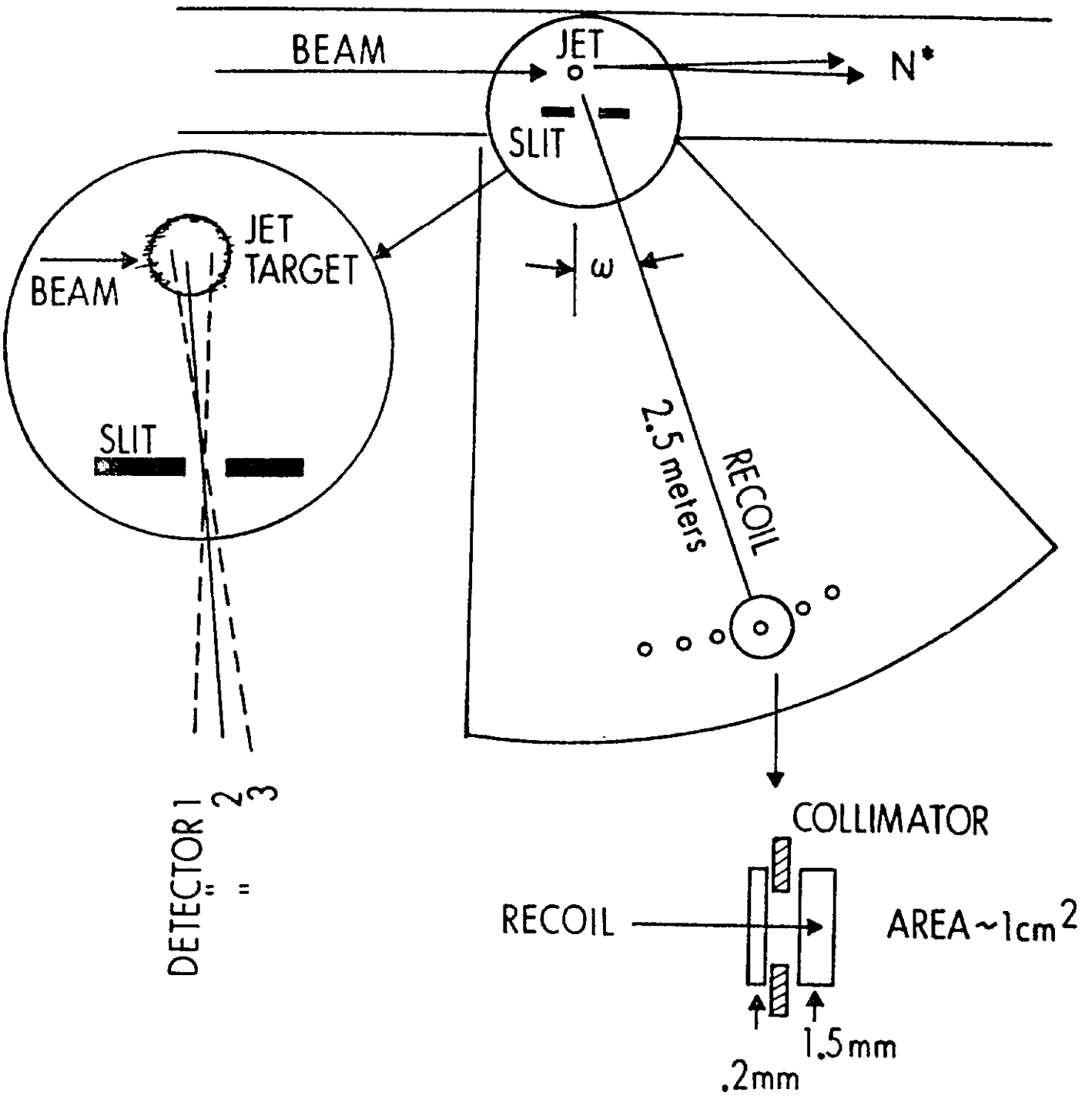
BEAM
JET
N*
SLIT
JET
TARGET
BEAM
SLIT
ω
2.5 meters
RECOIL
DETECTOR 1 2 3
COLLIMATOR
RECOIL
AREA ~ 1cm²
1.5mm
.2mm

Figure 1

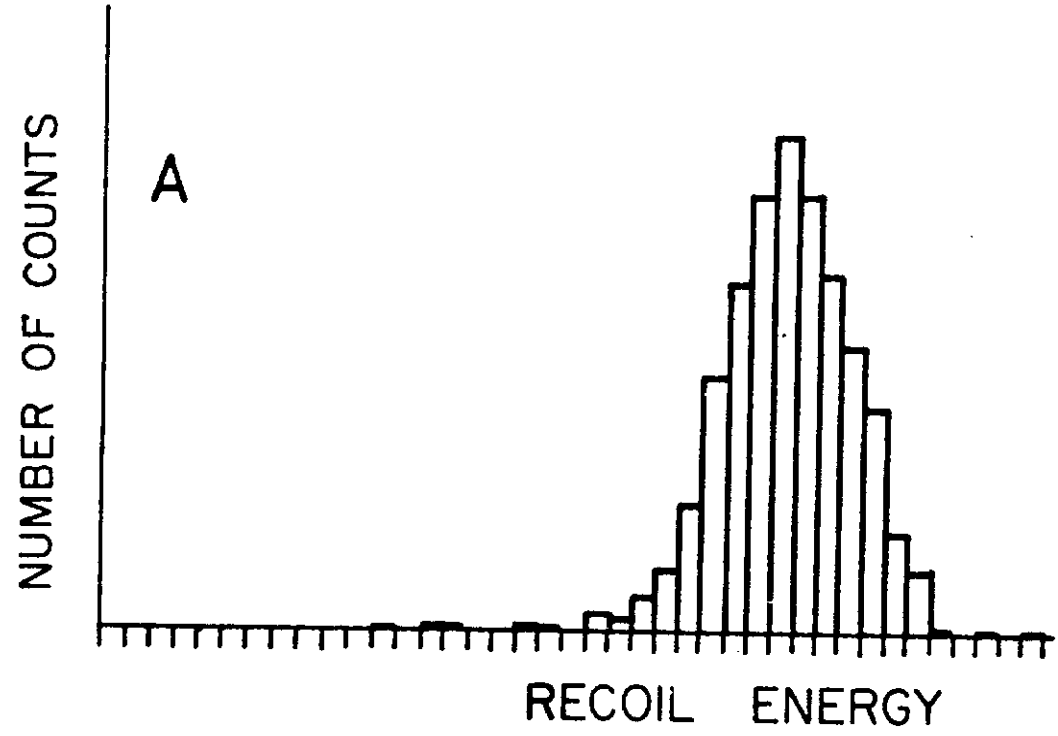
A
NUMBER OF COUNTS
RECOIL ENERGY

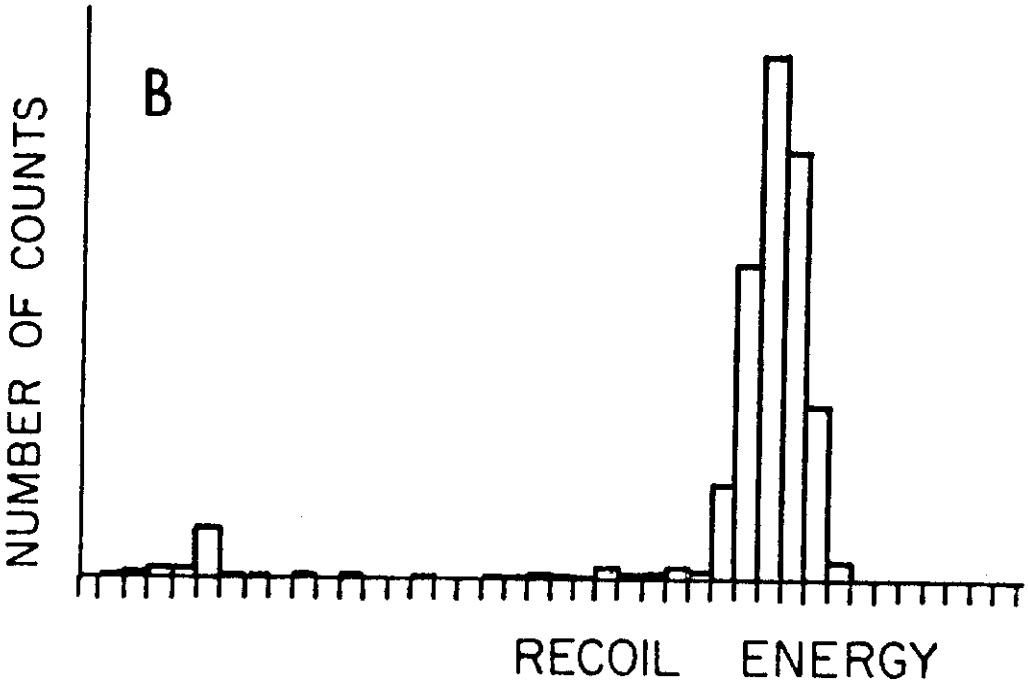
B
NUMBER OF COUNTS
RECOIL ENERGY

Fig 2

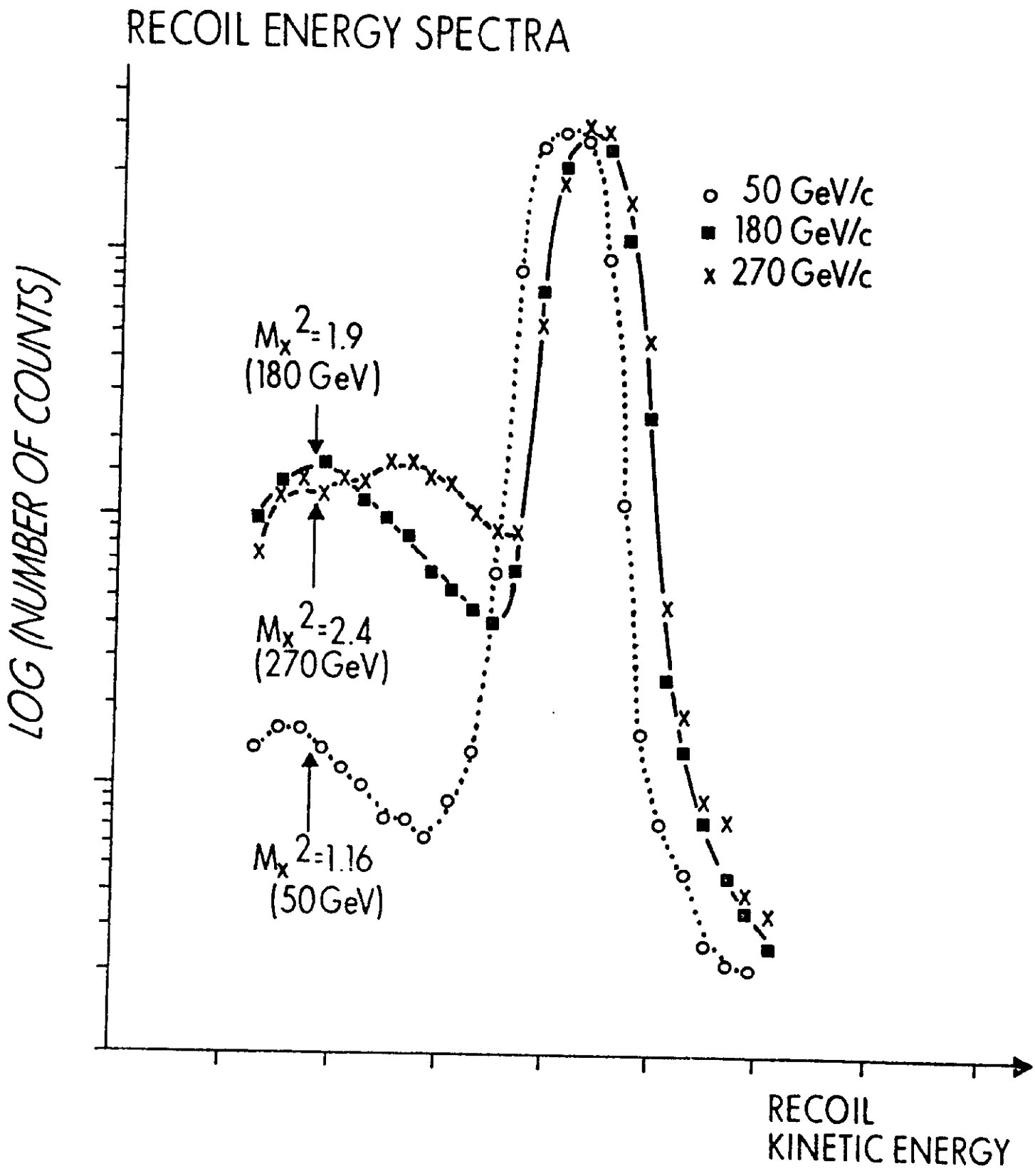
RECOIL ENERGY SPECTRA
LOG (NUMBER OF COUNTS)
50 GeV/c
180 GeV/c
270 GeV/c
M_x^2=1.9
(180 GeV)
M_x^2=2.4
(270GeV)
M_x^2=1.16
(50GeV)
RECOIL
KINETIC ENERGY

Figure 3

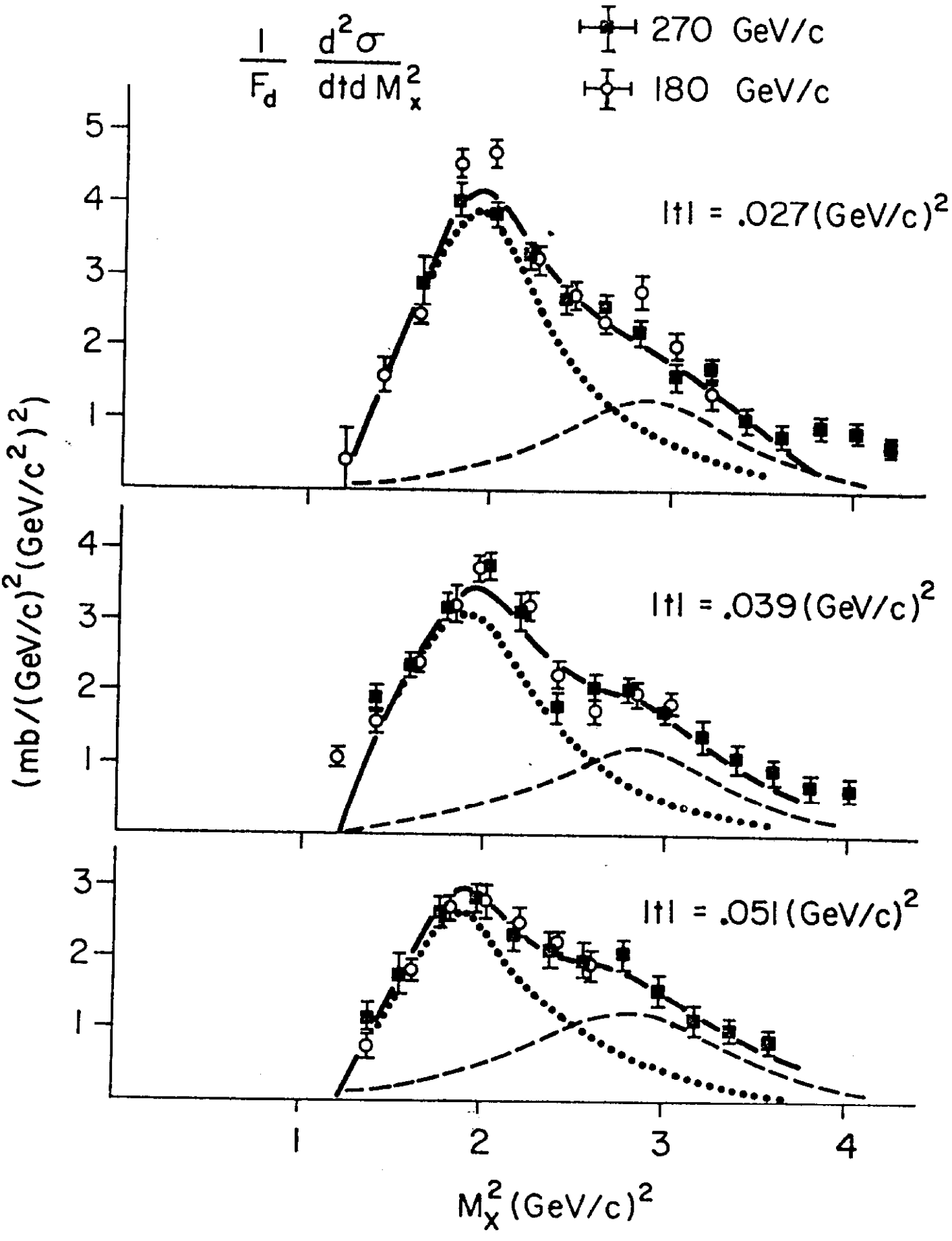
$\frac{1}{F_d}\frac{d^2\sigma}{dt\,dM_x^2}$
270 GeV/c
180 GeV/c
$|t| = .027 (GeV/c)^2$
$|t| = .039 (GeV/c)^2$
$|t| = .051 (GeV/c)^2$
$(mb/(GeV/c)^2 (GeV/c^2)^2)$
$M_x^2 (GeV/c)^2$

Figure 4

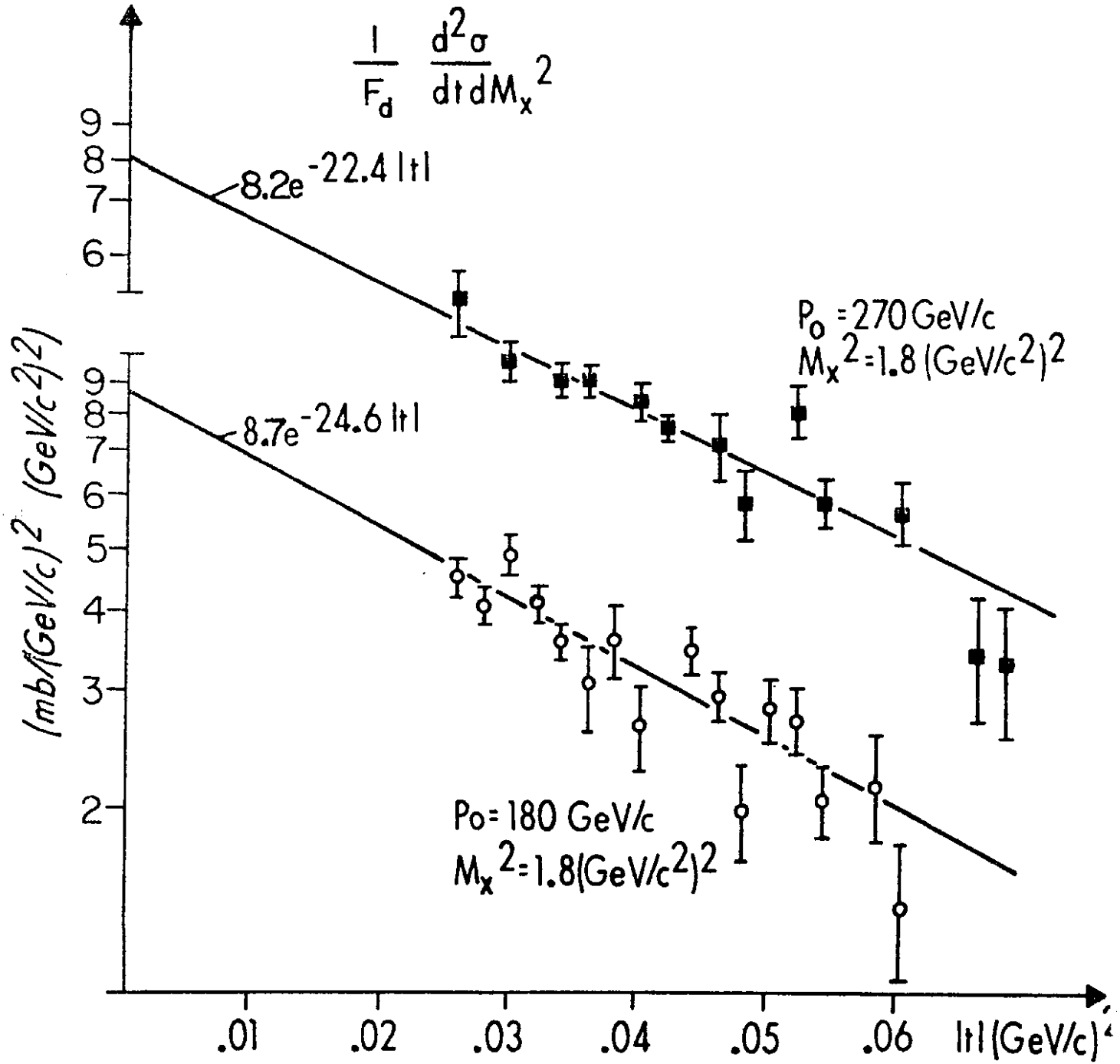
$\frac{1}{F_d}\frac{d^2\sigma}{dt\,dM_x^2}$
$8.2e^{-22.4|t|}$
$8.7e^{-24.6|t|}$
$P_o = 270$ GeV/c
$M_x^2 = 1.8$ (GeV/c^2)^2
$P_o = 180$ GeV/c
$M_x^2 = 1.8$(GeV/c^2)^2
(mb/(GeV/c)^2 (GeV/c^2)^2)
9
8
7
6
5
4
3
2
.01
.02
.03
.04
.05
.06
|t| (GeV/c)^2

Figure 5

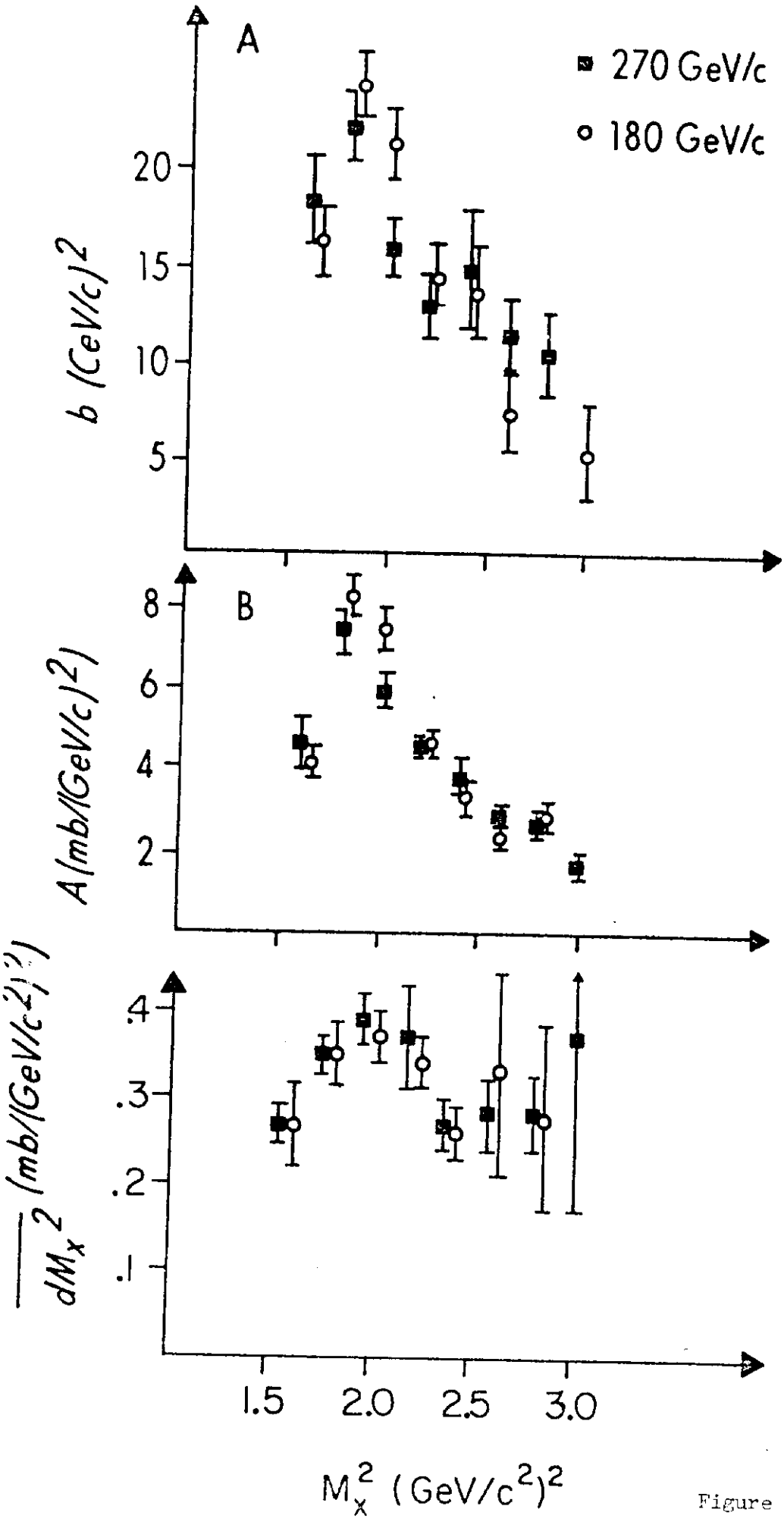
A
270 GeV/c
180 GeV/c
b (GeV/c)²
20
15
10
5
B
A (mb/(GeV/c)²)
8
6
4
2
dσ/dM_x² (mb/(GeV/c²)²)
.4
.3
.2
.1
1.5
2.0
2.5
3.0
M_x² (GeV/c²)²

Figure 6

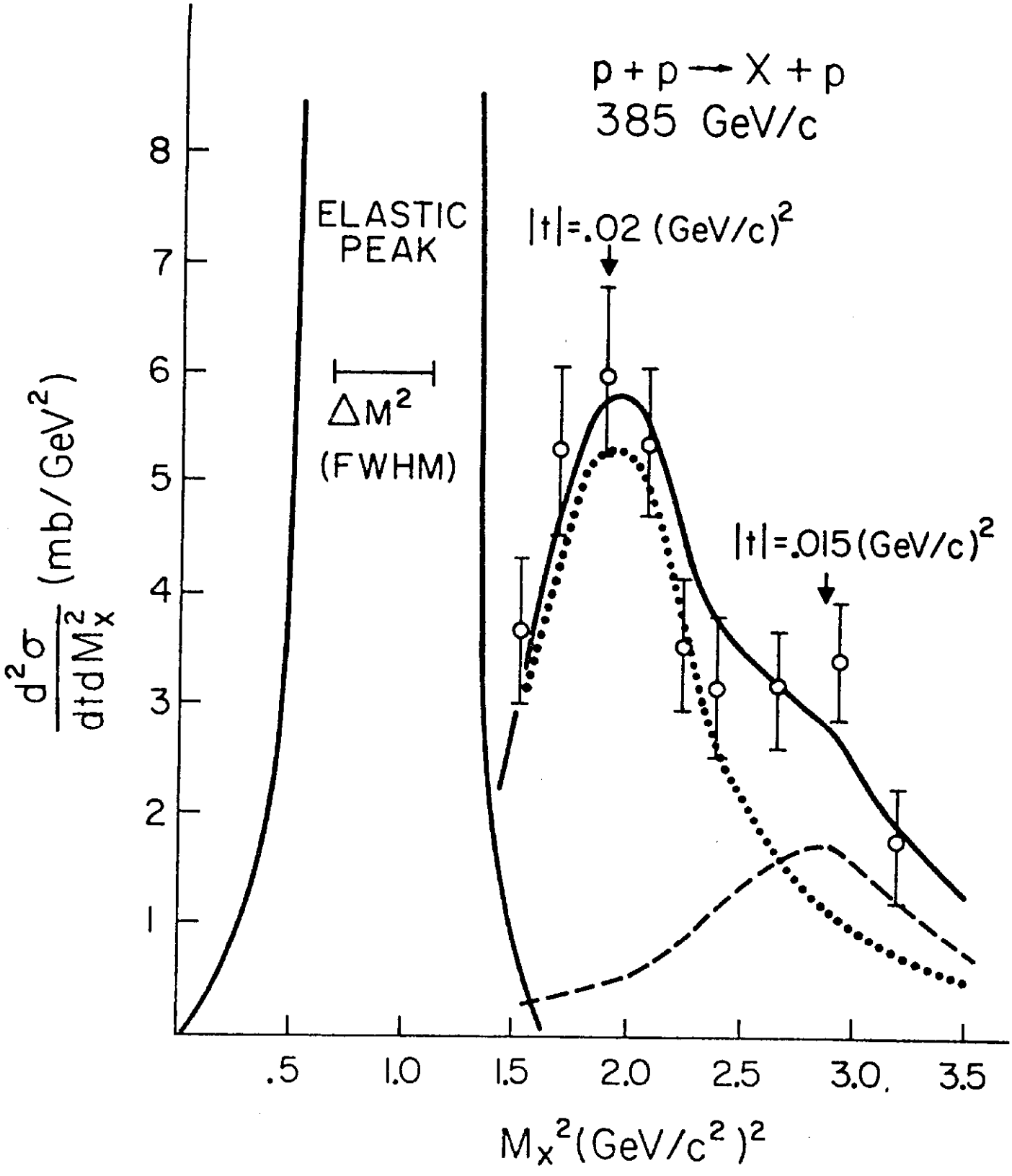
p + p → X + p
385 GeV/c
ELASTIC PEAK
ΔM² (FWHM)
|t|=.02 (GeV/c)²
|t|=.015 (GeV/c)²
d²σ/dtdM²x (mb/GeV²)
8
7
6
5
4
3
2
1
.5
1.0
1.5
2.0
2.5
3.0
3.5
Mx²(GeV/c²)²

Figure 7

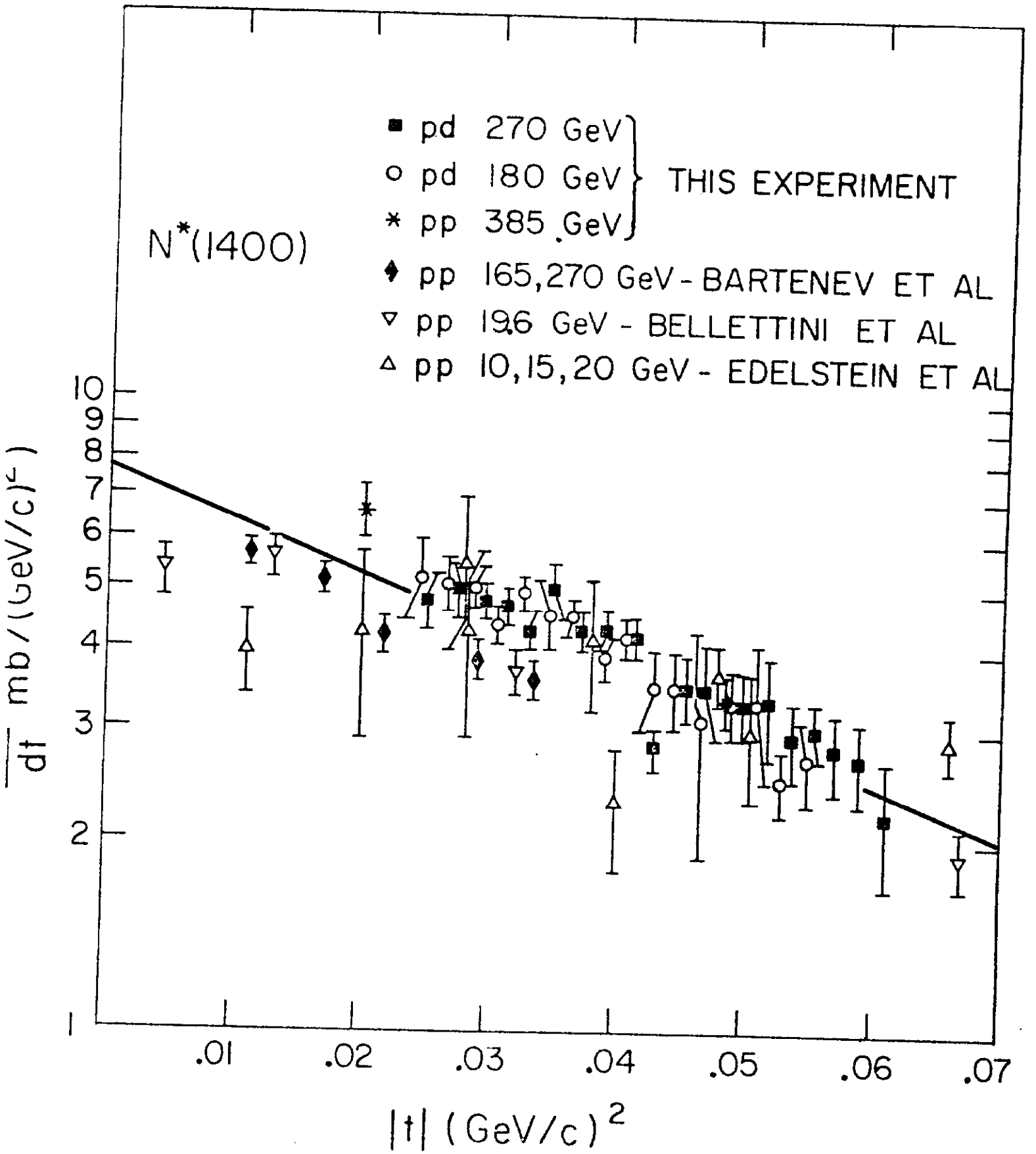
■ pd 270 GeV
○ pd 180 GeV
* pp 385 GeV
THIS EXPERIMENT
N*(1400)
♦ pp 165,270 GeV - BARTENEV ET AL
▽ pp 19.6 GeV - BELLETTINI ET AL
△ pp 10,15,20 GeV - EDELSTEIN ET AL
dt mb/(GeV/c)²
10
9
8
7
6
5
4
3
2
1
.01
.02
.03
.04
.05
.06
.07
|t| (GeV/c)²

Figure 3